Droplet growth by turbulent coagulation

By N. Riemer AND A.S. Wexler †

1. Motivation and objectives

Rain formation and the role of clouds in climate and atmospheric chemistry are closely linked to the evolution of the cloud droplet spectra. Our understanding of these processes is still fragmentary (Beard & Ochs 1993; Pinsky *et al.* 2000). This implies that the treatment of clouds leads to large uncertainties in weather and climate predictions.

Cloud droplets are initially produced by condensation of water vapor onto nuclei. Condensation alone, however, cannot form drops that are large enough to precipitate. In the absence of the ice phase this requires the coagulation of smaller droplets resulting in a larger drop. The process of coagulation relies on relative velocities between the droplet. One mechanism to provide relative velocities is the gravitational settling of the droplets. The larger droplets fall faster and collect smaller droplets on their way. However, this does not describe the real situation in a cloud sufficiently since the droplets are transported in a turbulent environment which results in relative velocities that will deviate from the mere differences of the terminal velocities in calm air.

Recent literature agrees that the in-cloud turbulence can enhance the collision kernel and hence the droplet growth significantly. However, the quantitative treatment of these processes represents a fundamental gap in our understanding of cloud microphysics. Although the potential importance of turbulence for droplet growth has been noted by Arenberg (1939) more than 60 years ago, progress has been slow in this area. At present, turbulence effects on cloud microphysics are ignored in most current cloud models.

Air turbulence in clouds can modify the collision process in at least four ways. First, particle inertia leads to increased relative velocities and less correlated velocity directions (acceleration effect). Second, the wind field shear produces collisions between particles even with the same inertia (shear effect). The acceleration and the shear effect are often referred to as the transport effect. Third, coagulation rates are enhanced due to local concentration increases for particle response times on the order of the Kolmorgorov scale. For this phenomenon the terms "preferential concentration" or "accumulation effect" have been coined. Fourth, turbulence can also impact the local droplet-droplet hydrodynamic interactions.

Since turbulence also influences the fields of temperature and water vapor it may impact condensational growth due to the turbulence induced fluctuations in supersaturation (see for instance the article by Paoli & Shariff (2004), this issue). This process, however, is beyond the scope of this paper.

Depending on the relation between the governing time scales of the fluid and the particle response times, the impact of the transport and accumulation effects varies. The transport effect is most dominant if the particle response time τ_p is on the order of the flow integral time scale T_e, whereas the accumulation effect is most dominant if τ_p is on the order of the Kolmogorov time scale τ_k (Wang *et al.* 2000; Reade & Collins 2000).

† Department of Mechanical and Aeronautical Engineering, University of California, Davis, U.S.A

Maxey (1987) first showed the phenomenon of preferential concentration, which was expanded by Squires & Eaton (1991) and Wang & Maxey (1993). Sundaram & Collins (1996) introduced the pair correlation function to quantify the effect of preferential concentration in the collision kernel. Since this work, further efforts have been made by Wang *et al.* (1998), Wang *et al.* (2000) and Zhou *et al.* (2001) to develop a model for the collision kernel on the basis of the solution of the Navier-Stokes equations using direct numerical simulations (DNS).

Pinsky & Khain (1997) brought the concept of preferential concentration to the atmospheric science community as a phenomenon that could play an important role in cloud microphysics. Indeed, several authors measured the existence of small-scale concentration fluctuations in clouds which strengthens the hypothesis that preferential concentration is also present in the atmosphere (Brenguier & Chaumat 2001; Kostinski & Shaw 2001).

Laboratory studies are rare compared to the theoretical ones, especially in the parameter range that relates to atmospheric clouds. Obviously, it is not feasible to cover the entire turbulent kinetic energy spectrum present in natural clouds with laboratory experiments. Woods *et al.* (1972), Jonas & Goldsmith (1972) and Neizvestny & Kobzunenko (1986) all conclude from their experiments that turbulence enhances drop collision. However, their experiments were limited to relatively small collector drops. Vohl *et al.* (1999) confirmed for larger collector drops that the droplets grow faster in turbulent flow compared to laminar flow.

As outlined in the brief literature review above, many of the theoretical studies have been devoted to the derivation of collision kernels. Few studies, however, investigate the resulting development of droplet size distributions (Park *et al.* 2002; Pinsky & Khain 1997). In light of the recent DNS-derived kernels we explore the possible impact of turbulence on the droplet size distribution for atmospheric conditions systematically, approaching the problem in two steps.

First, we will consider a Lagrangian box model of a cloud parcel simulating the evolution of the cloud droplet size distribution under the assumption that only coagulation is occuring. We will employ the coagulation kernel presented by Zhou *et al.* (2001), since their parameterization covers the accumulation and the transport effects. By applying this parameterization to atmospheric conditions, the potential influence of turbulent coagulation on droplet growth is evaluated.

In the second step, we will expand this model to a 1D-column model so that condensation, and transport processes such as turbulent diffusion and sedimentation can also be included.

In the following section the calculation of the turbulent collision kernel is outlined. Section 3 presents numerical results of the box model simulations, and Section 4 presents results of column model. Finally, future work is addressed in Section 5.

2. The collision kernel

Zhou *et al.* (2001) provide a model to predict the geometric collision kernel in a bidisperse system for a turbulent fluid, which is derived from DNS. This model includes both the turbulent transport effect and the accumulation effect. In this work we apply this kernel to calculate the development of cloud droplet spectra under atmospheric conditions. The following section outlines the calculation of the collision kernel in a turbulent fluid.

The ensemble average of the collision kernel $K_t(r_1, r_2)$ for two particles with radii r_1

and r_2 in a turbulent fluid can be expressed in a generalized form by Sundaram & Collins (1997):

$$K_t(r_1, r_2) = E_t \Gamma_0 \frac{\langle |w_r(r_1, r_2)| \rangle}{\langle |w_{r,\mathrm{shear}}(r_1, r_2)| \rangle} g_{12}(R), \tag{2.1}$$

where $R = r_1 + r_2$ is the collision radius and

$$\Gamma_0 = \sqrt{\frac{8\pi}{15}} R^3 \frac{v_k}{\eta} \tag{2.2}$$

is the collision kernel for zero-inertia particles according to Saffman & Turner (1956), with the Kolmogorov velocity scale $v_k = (\nu\epsilon)^{\frac{1}{4}}$, where ν is the kinematic viscosity of the fluid and ϵ is the dissipation rate. The Kolmogorov length scale is $\eta = (\nu^3/\epsilon)^{\frac{1}{4}}$, and E_t is the turbulent collection efficiency. The notation $\langle |w_r(r_1, r_2)| \rangle$ denotes the ensemble-averaged magnitude of the relative velocity of particles with radii r_1 and r_2.

The collection efficiency E_t is defined as the product of the collision efficiency $E_{\mathrm{col},t}$ and the coalescence efficiency $E_{\mathrm{coa},t}$. The collision efficiency represents the ratio of the actual number of collisions to the number for complete geometric sweep-out. However, collision does not guarantee coalescence. The coalescence efficiency accounts for this fact and is defined as the ratio of the number of coalescences to the number of collisions.

The hydrodynamic interactions of droplets in turbulent flow are highly uncertain, but there are indications that the collision efficiency is larger in turbulence than in calm air (Pinsky *et al.* 1999). In our study we retain the value $E_{\mathrm{col},t} = 1$. An estimation of the impact of $E_{\mathrm{col},t} < 1$ based on the work of Pinsky *et al.* (1999) is given in Riemer & Wexler (2004).

Even less is known about the coalescence efficiency in turbulent flow, $E_{\mathrm{coa},t}$. Laboratory studies of small colliding droplets show that the coalescence efficiency is close to 1 if the droplets are charged and an electrical field is present (Rogers & Yau 1989). Because weak fields and charges exist in natural clouds, we therefore assume $E_{\mathrm{coa},t} = 1$ for the sake of simplicity.

The term $\langle |w_r(r_1, r_2)| \rangle / \langle |w_{r,\mathrm{shear}}(r_1, r_2)| \rangle$ with its two components – shear and acceleration – represents the turbulent transport effect by

$$\begin{aligned} \langle |w_{r,\mathrm{shear}}(r_1, r_2)| \rangle &= \sqrt{\tfrac{2}{15\pi}} v_k \frac{R}{\eta}, \qquad \frac{\langle |w_r(r_1,r_2)| \rangle}{\langle |w_{r,\mathrm{shear}}(r_1,r_2)| \rangle} = \left[1 + 15 \frac{w_{r,\mathrm{accel}}^2}{v_k^2} \left(\frac{\eta}{R}\right)^2\right]^{\frac{1}{2}} \\ \frac{w_{r,\mathrm{accel}}^2}{v_k^2} &= C_w(\phi) \left(\frac{u'}{v_k}\right)^2 \frac{\gamma}{\gamma - 1} \left((\theta_1 + \theta_2) - \frac{4\theta_1\theta_2}{(\theta_1+\theta_2)} \sqrt{\frac{1+\theta_1+\theta_2}{(1+\theta_1)(1+\theta_2)}}\right) \times \\ &\qquad \left[\frac{1}{(1+\theta_1)(1+\theta_2)} - \frac{1}{(1+\gamma\theta_1)(1+\gamma\theta_2)}\right], \end{aligned} \tag{2.3}$$

where $\theta_i = 2.5\tau_p(r_i)/T_e$ $(i = 1, 2)$ is proportional to the ratio of particle response time $\tau_p = 2\rho_p r_i^2/(9\nu\rho)$ to flow integral time $T_e = u'^2/\epsilon$. Here, ρ_p is the particle density, ρ the fluid density, r_i particle radius and u' the fluid r.m.s. velocity fluctuation.

Equation (2.3) is developed on the basis of the formulation by Kruis & Kusters (1997). To fit their numerical results, Zhou *et al.* (2001) introduced the function $C_w(\phi) = 1.0 + 0.6 \exp\left[-(\phi - 1)^{1.5}\right]$ and the factor $\gamma = \phi \times 0.183 u'^2/\sqrt{\epsilon\nu}$ with $\phi = \max(\theta_2/\theta_1, \theta_1/\theta_2)$.

The factor

$$g_{12}(R) = 1 + \rho_{12} \sqrt{g_{11}(R) - 1} \sqrt{g_{22}(R) - 1} \tag{2.4}$$

is the bidisperse radial distribution function at contact and accounts for the accumulation

$$
\begin{aligned}
y_0(\alpha) &= 18\alpha^2 \\
y_1(\alpha) &= 0.36\alpha^{2.5}\exp(-\alpha^{2.5}) \\
y_2(\alpha) &= 0.24\exp(-0.5\alpha) \\
y_3(\alpha) &= 0.013\exp(-0.07\alpha) \\
z_0(\alpha) &= \tfrac{1}{2}\left[1+\tanh\tfrac{\alpha-0.5}{0.25}\right] \\
z_1(\alpha) &= \tfrac{1}{2}\left[1+\tanh\tfrac{\alpha-1.25}{0.1}\right] \\
z_2(\alpha) &= \tfrac{1}{2}\left[1+\tanh\tfrac{\alpha-6.5}{2.5}\right]
\end{aligned}
$$

TABLE 1. Auxiliary functions for the radial distribution function g_{ii}

effect, which is governed by the monodisperse radial distribution functions g_{ii} (i=1,2; no summation implied) and the concentration correlation coefficient

$$\rho_{12} = 2.6\exp(-\psi) + 0.205\exp(-0.0206\psi)\frac{1}{2}(1+\tanh(\psi-3)). \tag{2.5}$$

where $\psi = \max(\tau_{p2}/\tau_{p1}, \tau_{p1}/\tau_{p2})$ and

$$g_{ii} = 1 + y_0(\alpha)[1-z_0^2(\alpha)] + R_\lambda z_0^2(\alpha)\{y_1(\alpha)[1-z_1(\alpha)] + y_2(\alpha)z_1(\alpha) + y_3(\alpha)z_2(\alpha)\}. \tag{2.6}$$

The functions $y_0(\alpha)$, $y_1(\alpha)$, $y_2(\alpha)$, $y_3(\alpha)$, $z_0(\alpha)$, $z_1(\alpha)$ and $z_2(\alpha)$ are given in Table 1. Here, the argument $\alpha = \tau_{pi}/\tau_k$ is the Stokes number where $\tau_k = \sqrt{\nu/\epsilon}$ is the Kolmogorov time scale.

The monodisperse radial distribution function g_{ii} scales with the Taylor-microscale Reynolds number, which is defined as $R_\lambda = u'\lambda/\nu$ with the transverse Taylor microscale $\lambda = \sqrt{15\nu u'^2/\epsilon}$. The linear dependence of g_{ii} on R_λ is based on the results of DNS, which only cover a range of low Reynolds numbers compared to atmospheric conditions. The extrapolation of this relationship to high Reynolds numbers introduces some uncertainty which we must keep in mind when interpreting our results.

Zhou *et al.* (2001) employ furthermore the following assumptions in their model: The size of the particles is on the order of or less than the Kolmogorov length scale η. The particle volume fraction and mass loading are sufficiently low so that the presence of the particles does not impact the gas turbulence. These assumptions are valid for clouds as established in Section 2.1.

Moreover, their DNS do not include the effect of gravity. In the atmosphere, clearly both turbulence and gravitation effect the size distribution. Therefore it is necessary to formulate a collision kernel that includes both mechanisms. The usual approach for modeling the impact of several coagulation mechanisms, for instance Brownian motion and gravitational settling, is simply adding the individual kernels. As Butuirat & Kielkiewicz (1996) show this method gives satisfactory results. However if the accumulation effect is also involved, the formulation of the resulting kernel requires more caution because sedimentation might counteract the clustering effect (Vaillancourt & Yau 2000). The overall effect of the interaction of gravitation and turbulence on the coagulation of particles is still not very well understood at this stage and represents an area where further research is needed.

Unless otherwise indicated, we will consider the effect of gravity and turbulence separately. To estimate the interaction of these processes, we simply add the turbulent and

sedimentation kernels. Clearly, this approach is only preliminary and will be improved as research progresses.

In our investigation the sedimentation kernel $K_s(r_1, r_2)$ for calm air will be employed for comparison, which is given by:

$$K_s(r_1, r_2) = \pi(r_1 + r_2)^2 E_s |v_T(r_1) - v_T(r_2)|. \tag{2.7}$$

Here, E_s is the collision efficiency for calm air for which we use the values provided by Hall (1980), and $v_T(r_1)$, $v_T(r_2)$ are the terminal velocities of the droplets in calm air.

2.1. *Calculation of the size distributions*

The stochastic collection equation describes the evolution of a colliding and coalescing cloud droplet size distribution (Pruppacher & Klett 1997):

$$\begin{aligned} \frac{\partial n(m,t)}{\partial t} &= \tfrac{1}{2} \int_{m_0}^{m} n(m_c, t) K(m_c, m') n(m', t) dm' \\ &\quad - \int_{m_0}^{\infty} n(m, t) K(m, m') n(m', t) dm', \end{aligned} \tag{2.8}$$

where $n(m,t)$ is the drop number distribution function at time t and $K(m_c, m')$ is the collection kernel describing the rate at which a droplet of mass $m_c = m - m'$ is collected by a droplet of mass m' forming a droplet of mass m. The following transformation of variables leads to the stochastic collection equation for the mass size distribution $g(y,t)$ (Berry 1967):

$$g(y,t)dy = m\, n(m,t) dm, \quad n(m,t) = \frac{1}{3m^2} g(y,t), \tag{2.9}$$

where $y = \ln r$, and r is the radius of droplets with mass m.

$$\begin{aligned} \frac{\partial g(y,t)}{\partial t} &= \tfrac{1}{2} \int_{y_0}^{y} \tfrac{m^2}{m_c^2 m'} g(y_c, t) K(y_c, y') g(y', t) dy' \\ &\quad - \int_{y_0}^{\infty} g(y,t) \tfrac{K(y,y')}{m'} g(y', t) dy'. \end{aligned} \tag{2.10}$$

As the initial cloud droplet distribution we use a Gamma function of the form $n(m, t = 0) = L_w / \bar{m}^2 \exp(-m/\bar{m})$, where L_w is the total cloud water content, and $\bar{m}$ is the mean droplet mass. Assuming spherical droplets, $\bar{m}$ and the mean droplet radius $\bar{r}$ are related by $\bar{m}(r) = 4/3\pi\rho_p \bar{r}^3$, where ρ_p is the water density.

For our simulations, L_w is set to 1 g m^{-3}, typical for warm rain clouds and $\bar{r}$ to 10 μm, a typical cloud droplet size. This means that the assumptions mentioned above (low mass loading and particles smaller than or on the order of η) hold. Solution of the stochastic collection equation (2.10) uses the flux method by Bott (1998), which has been proved to be both efficient and mass conservative. For the collection kernel K we employ the turbulent collision kernel K_t as described in Section 2 for different atmospheric conditions and compare the results to those obtained with the kernel for sedimentation in calm air K_s (equation (2.7)).

Cloud dissipation rates ϵ depend on cloud type and age. The values range from 10 cm^2 s^{-3} for stratus clouds to several 100 cm^2 s^{-3} for cumili and 1000 cm^2 s^{-3} for cumulonimbus clouds (Pruppacher & Klett 1997).

Figure 1 shows measured dissipation rates ϵ in clouds with the corresponding r.m.s. velocity u' (MacPherson & Isaac 1977). From dimensional arguments, a cubic relation

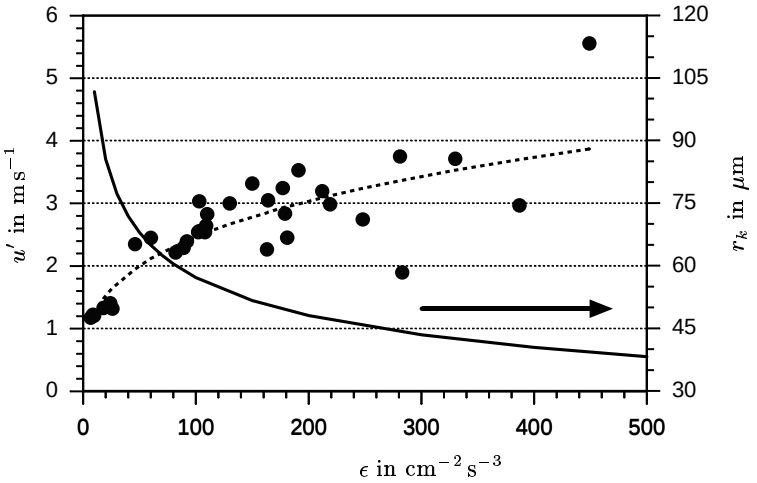

FIGURE 1. Full circles: Measured values of u' and ϵ in clouds (MacPherson & Isaac 1977), dashed line: fit of measured data, solid line: particle radius for which $\tau_p = \tau_k$ (see text for details).

between ϵ and u' is expected, since

$$\epsilon = \frac{u'^3}{L}, \tag{2.11}$$

as long as the characteristic length scale L is relatively constant. The dashed line shows the fit to the data points for $L = 1500$ m. The solid line shows the radius r_k that fulfills the condition $\tau_p(r_k) = \tau_k(\epsilon)$, showing that the accumulation effect is important.

Clearly, for values of ϵ that occur in the atmosphere, the values for r_k are in the range of observed cloud droplet sizes. Therefore the accumulation effect is expected to be significant for droplets between 30 μm and 100 μm. The transport effect, however, is less important since $\tau_p = T_e$ applies for unreasonably large particle sizes under atmospheric conditions.

In the following, the values of $\epsilon = 300$ cm^2 s^{-3} and $u' = 3.5$ m s^{-1} are used for the base case, which fulfill equation (2.11) and represent in-cloud turbulence of moderate to high intensity.

3. Box model simulations

In this section we evaluate the influence of turbulence on the evolution of the drop size spectra if only coagulation is considered. Figure 2a shows the turbulent coagulation kernel K_t according to equation (2.1) for the base case, and figure 2b shows the relative differences $(K_t - K_s)/K_s$ to the sedimentation kernel K_s according to equation (2.7). Given equation (2.7), it is clear that K_s depends both on the absolute and on the relative particle sizes. In particular, since it depends on the relative velocity it becomes large if the sizes of the colliding droplets are different and zero for equally sized droplets. The turbulent coagulation kernel K_t exhibits a distinct local maximum for the combination of droplet radii near 65 μm and 250 μm using the base case values for ϵ and u'. The exact position as well as the magnitude of this maximum depend on ϵ and u'. It shifts to larger radii for smaller dissipation rates, which means that higher dissipation rates enhance the coagulation process at an earlier stage. Note that the local maximum in the 65 to 250 μm size range is not of primary importance for the onset of effective coagulation.

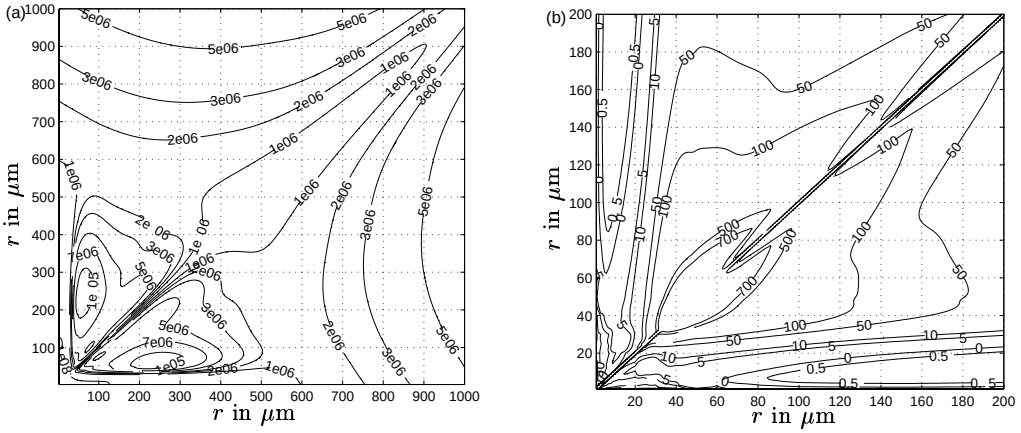

FIGURE 2. (a) K_t in $\mathrm{m^3\,s^{-1}}$ for $\epsilon = 300\ \mathrm{cm^2\,s^{-3}}$ and $u' = 3.5\ \mathrm{m\,s^{-1}}$. (b) Relative differences $(K_t - K_s)/K_s$. K_t as in figure 2. Note the different scale of the axis compared to figure 2a.

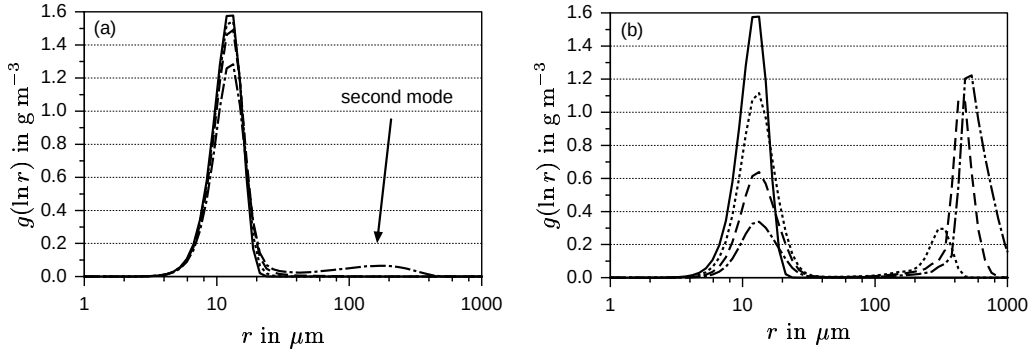

FIGURE 3. (a) Temporal evolution of the mass size distribution with sedimentation kernel according to Hall (1980). (b) Same as (a) but with turbulent kernel (base case). ——— : start, · · ·: 10 min., – – – – : 20 min., — · —: 30 min.

To be effective, turbulent coagulation must help particle grow through the 10-40 μm gap. Below this size range condensation grows particles effectively, above this size range settling coagulation becomes an effective mechanism for particle growth. Indeed figure 2 shows that K_t is by about a factor of 5-10 larger than K_s in this size range. Moreover, turbulent coagulation is also effective for same-sized particles.

We can therefore expect that the impact of turbulent coagulation is especially significant in the initial stage of the development of the cloud whereas the impact decreases for large cloud droplets or rain drops.

Figure 3 shows the temporal evolution of the mass distribution $g(\ln r)$ for the sedimentation kernel and for the turbulent kernel for the base case. For the sedimentation kernel (figure 3a) a second mode appears only after about 30 minutes. At $t = 30$ min, most of the mass (97 %) is still distributed over the droplet size range smaller than 100 μm, confirming the well known fact that sedimentation alone cannot explain the fast formation of large droplets. For the turbulent kernel (figure 3b), the second mode forms already after 10 minutes, because the turbulent coagulation kernel of Zhou *et al.* (2001) accelerates the formation of large drops. For simulation times around one hour, the sedimentation and

turbulent kernels predict similar distributions, supporting the finding that turbulence is especially important for the early stage of the development of the cloud. If the combined sedimentation and turbulent kernel is considered, the second mode becomes visible after only 5 minutes, and after 30 minutes 96 % of the mass is transferred to sizes larger than 100 μm (not shown here).

The temporal evolution of the size distribution shows a strong sensitivity to the dissipation rate. We will address this point in section 4.

4. 1D simulations

With the boxmodel presented in section 3 only the impact of coagulation has been studied and we found that turbulent coagulation can accelerate rain formation significantly. In the real atmosphere, however, condensation is also an important process – in fact condensation is the governing process in the early stage of droplet growth. Additionally, transport processes such as turbulent diffusion and sedimentation take place. The question arises if the result of the previous section still holds considering the interaction of these processes.

To address this question, we consider a column of air parcels with a prescribed aerosol distribution that undergoes an updraft (e.g. cooling) process. For the set up of the base case and the initial condition see table 2.

The size distribution of the aerosol particles (solid line in figure 4a) is initially prescribed in each grid box. We use 100 logarithmically spaced bins to discretize the size distribution with respect to radius. At the start of the simulation the water content of the aerosol particles is calculated according to equilibrium conditions assuming that the aerosol consists of ammonium sulfate. As a consequence of the ascent of the column supersaturation is reached and a proportion of the aerosol particles are activated serving as cloud condensation nuclei (CCN). The processes of condensation/evaporation, coagulation, turbulent diffusion and sedimentation shape the size distribution and feed back on the supersaturation of the system. We assume a constant updraft velocity and do not consider entrainment processes.

The following set of equations describes the system: As the column rises, the potential temperature θ and the specific humidity q change according to:

$$\frac{\partial \theta}{\partial t} = \frac{\partial}{\partial z}\left(K_h \frac{\partial \theta}{\partial z}\right) - \left(\frac{p_0}{p}\right)^{0.286} \frac{L_v}{c_{pa}\rho}\left(\frac{\partial}{\partial t} q\right)_{\text{phase}}, \tag{4.1}$$

$$\frac{\partial q}{\partial t} = \frac{\partial}{\partial z}\left(K_h \frac{\partial q}{\partial z}\right) + \frac{1}{\rho}\left(\frac{\partial}{\partial t} q\right)_{\text{phase}}. \tag{4.2}$$

Here K_h is the eddy diffusivity for heat, c_{pa} is the specific heat of dry air at constant pressure, L_v is the latent heat of condensation, p is the pressure, and ρ is the air density.

Changes of the size distribution of the water mass g_w are calculated as follows:

$$\begin{aligned}\frac{\partial g_w}{\partial t} = &\frac{\partial}{\partial z}\left(K_h \frac{\partial g_w}{\partial z}\right) - \frac{\partial}{\partial z}\left(v_t g_w\right) \\ &+ H g_w - \frac{1}{3}\frac{\partial}{\partial y}(H g_w) + \left(\frac{\partial g_w}{\partial t}\right)_{\text{coa}}\end{aligned} \tag{4.3}$$

The last term corresponds to coagulation and is defined in equation (2.10). The second term of the right hand side describes sedimentation with terminal velocity v_t.

Updraft velocity	1 ms^{-1}
Vertical gridsize	20 m
Total column height	500 m
Initial aerosol distribution	see figure 4
Eddy diffusivity	10 $\mathrm{m}^2\mathrm{s}^{-1}$
Dissipation rate	300 $\mathrm{cm}^2\mathrm{s}^{-3}$
r.m.s. velocity	3 ms^{-1}
Relative humidity	from 91 % (layer 1, bottom) increasing to 99.6 % (layer 25, top)
Temperature	from 285 K (layer 1) decreasing with wet-adiabatic lapse rate

TABLE 2. Model parameters and initial conditions

The third and fourth terms specify the condensation/evaporation with the condensation/evaporation rate H defined as

$$H = \frac{1}{m(r)} \frac{\partial m(r)}{\partial t} \tag{4.4}$$

here m is the mass of a particle of size r.

The growth rate $\partial m/\partial t$ of the particles is calculated according to Majeed and Wexler (2001).

$$\frac{\partial m(r)}{\partial t} = \frac{4\pi r D_v' M_w p^\circ(T)/(RT)\,[\mathrm{RH} - \exp(\mathrm{A} - \mathrm{B})]}{1 + (4\pi r D_v' M_w p^\circ(T)/(RT))(L_v M_w/(RT))(L_v/(4\pi r k_a' T))\exp(A - B)},$$

with

$$A = \frac{2 M_w \sigma_w}{R T_a \rho_w r}, \quad B = \nu_m \frac{M_w}{M_s} \frac{m_s}{m_d - m_p}, \tag{4.5}$$

where M_w is the molecular weight of water vapor, M_s the molecular weight of the solute, R the universal gas constant, D_v' the water diffusivity corrected for non-continuum effects, T the temperature of the environment, T_a the droplet temperature, $p^\circ(T)$ the water saturation pressure at T, RH the relative humidity, L_v the latent heat of water, k_a' the thermal conductivity corrected for non-continuum effects, σ_w the air-water surface tension, ρ_w the water density, ν_m the number of ions per solute molecule, m_s, m_d and m_p the masses of solute, droplet and dry particle.

A corresponding equation can be formulated for the aerosol mass distribution. Since we do not consider chemical processes the terms for condensation/evaporation vanish.

$$\frac{\partial g_a}{\partial t} = \frac{\partial}{\partial z}\left(K_h \frac{\partial g_a}{\partial z}\right) - \frac{\partial}{\partial z}\left(v_t g_w\right) + \left(\frac{\partial g_a}{\partial t}\right)_{\mathrm{coa}} \tag{4.6}$$

The term due to the phase change of water vapor in equations 4.1 and 4.2 may be obtained by integrating over the whole droplet spectrum :

$$\left(\frac{\partial q}{\partial t}\right)_{\mathrm{phase}} = \int_0^\infty H g_w - \frac{1}{3}\frac{\partial}{\partial y}(H g_w)\mathrm{d}y \tag{4.7}$$

For solving these equations we apply operator splitting. The terms for turbulent diffu-

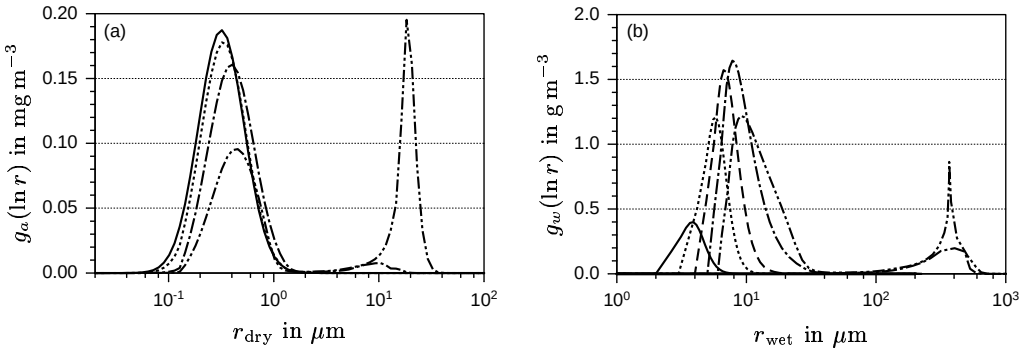

FIGURE 4. (a) Temporal development of the dry aerosol mass size distribution, layer 6, base case. ——— : start, · · ·: 15 min., — · —: 25 min., — · · —: 30 min. (b) Same as figure 4a but for water mass size distribution. ——— : 7 min., · · ·: 15 min., - - - - : 20 min., — · —: 25 min., — · · —: 30 min.

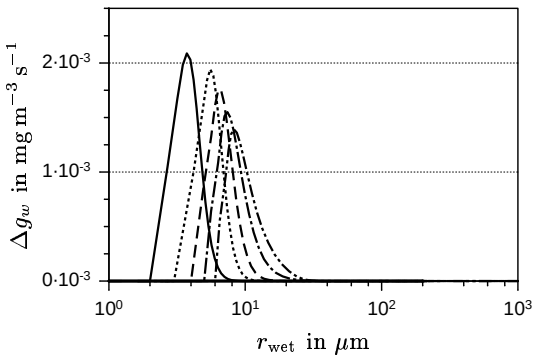

FIGURE 5. Rates of change of the water mass size distribution due to condensation. ——— : 7 min., · · ·: 15 min., - - - - : 20 min., — · —: 25 min., — · · —: 30 min.

sion are solved with an implicit scheme, for the sedimentation terms we use the advection algorithm according to Dhaniyala & Wexler (1996).

Coagulation is treated as following: For the dry aerosol mass we use a fixed grid with respect to the dry particle radius and apply the method by Bott (1998). The associated water is moved from bin to bin accordingly assuming an internal mixture of the whole droplet.

For the condensation of water we use a moving grid. The advantage of this hybrid approach (e.g. fixed grid for coagulation, moving grid for condensation) is that it avoids numerical diffusion as it occurs when treating condensation on a fixed grid. It also ensures that the aerosol mass is regenerated after evaporation, which is important for the investigation of aerosol processing.

Figure 4a shows the temporal development of the dry aerosol mass size distribution in layer 6 for the base case. Starting from the initial distribution, the dry aerosol mass is transferred to larger radii over the course of the simulation due to the coagulation process. The corresponding development of the water mass distribution in figure 4b shows that large droplets are formed after 25 min. To understand the development of the size distribution it is necessary to analyse which process is most important at various

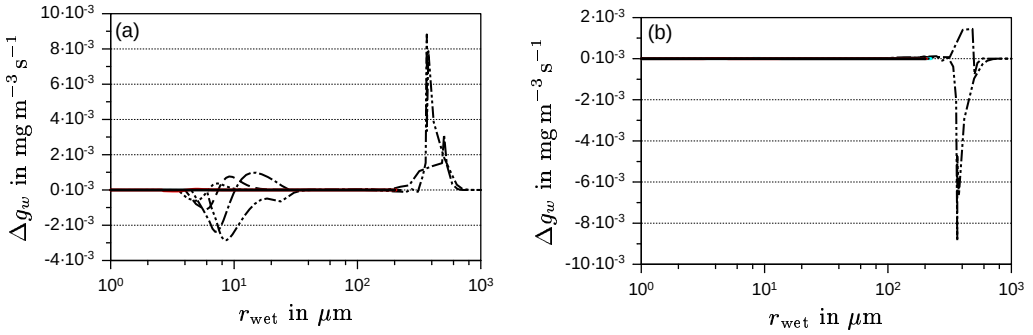

FIGURE 6. (a) Rates of change of the water mass size distribution due to coagulation. (b) Same as (a) but for sedimentation. ——— : 7 min., ···: 15 min., - - - - : 20 min., — · —: 25 min., — · · —: 30 min.

times over the course of the simulation. Figure 5 and 6 display these processes for this purpose. As seen from figure 5 condensation is dominant for the size range below 20 μm and therefore most important for the early stages of the simulation. Figure 6a shows that after 25 min. coagulation takes over and shifts the mass from sizes below 20 μm to those above 100 μm. As seen in figure 6b sedimentation becomes important once the droplets have attained a critical size of about 300 μm. This process eventually removes the water and associated CCN from the column.

Figure 7a shows the sensitivity towards the turbulence intensity. All size distributions are shown at t=30 min. The case without turbulent coagulation (coagulation only due to sedimentation) is included for comparison. For this case we see the results of the box model study confirmed. The size distribution is still very narrow and does not show any formation of larger size droplets. For $\epsilon = 100$ cm^2 s^{-3} the second maximum is not apparent, but a broadening towards the right is noticable. For both $\epsilon = 300$ cm^2 s^{-3} and $\epsilon = 500$ cm^2 s^{-3} large droplets are formed. For $\epsilon = 500$ cm^2 s^{-3} the formation occurs already ealier in the simulation so that at t=30 min. more water mass has been removed from the column due to sedimentation.

Finally we want to address the uncertainty concerning the Reynolds number dependence of the coagulation kernel. As mentioned in section 2 some uncertainty is introduced in the calculation of the coagulation kernel since we assume that the radial distribution function g_{12} depends linearly on the Reynolds number. While this assumption holds for the range of Reynolds numbers that are covered in DNS, it is unknown if this would still be the case for Reynolds numbers in the atmosphere or if g_{12} would level off after some (likewise unknown) threshold value is reached. Such behavior has been found for other problems in turbulence. For instance Belin *et al.* (1997) have shown for the velocity gradient distributions in turbulence that a change in the dependence of the parameters of the distributions on the Reynolds number can be found around $R_\lambda = 700$. To estimate the sensitivity in our model we carry out an additional simulation where R_λ in equation (2.6) is set artificially to 700 while ϵ and u' are set to the base case values. The result in figure 7b shows that compared to figure 4b, the development of large droplets is clearly delayed. However, compared to the case with coagulation due to sedimentation only strong acceleration of the large droplet formation within the first 30 min. can still be noticed.

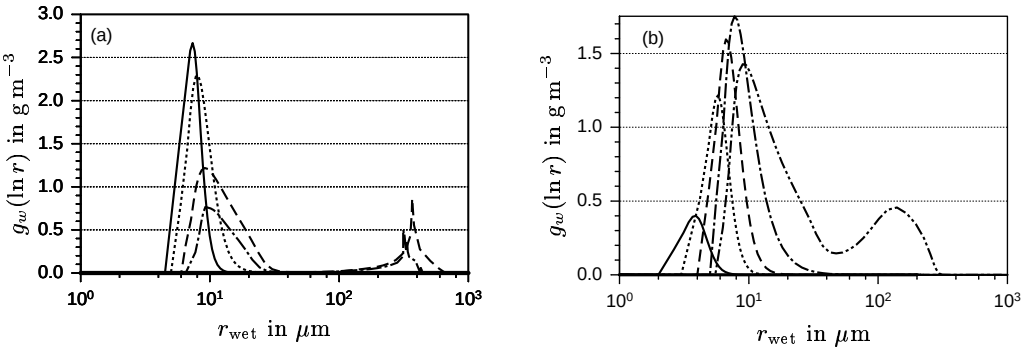

FIGURE 7. (a) Size distribution of water mass for different dissipation rates, t = 30 min. ——— : no turbulence, $\cdots$: 100 cm^2 s^{-3}, – – – – : 300 cm^2 s^{-3}, – · –: 500 cm^2 s^{-3}. (b) Temporal development of the water mass size distribution with R_λ set to 700. ——— : 7 min., $\cdots$: 15 min., – – – – : 20 min., – · –: 25 min., – · · –: 30 min.

5. Conclusions and future work

In this paper we have investigated the impact of turbulence on the development of cloud droplet spectra. In a two-step approach we have shown first that – compared to the effect of sedimentation in calm air only – even moderate turbulence can enhance the formation of large droplets significantly. The largest impact of turbulence is expected for similar sized particles and/or for particles in the size range smaller than 100 μm. Here, the collision kernel is enhanced by several orders of magnitude if turbulence is included, which accelerates the growth of droplets dramatically. By treating coagulation, condensation, turbulent diffusion and sedimentation in a 1D model we find the result confirmed. Turbulent coagulation appears to be the key mechanism that bridges the gap in transforming droplets into drops.

This model framework represents a powerful tool to investigate the impact of in-cloud turbulence on the various interactions of clouds and the Earth system. The validation of the model with observational data is currently underway.

Further plans should address the interaction of cloud microphysics with in-cloud chemistry. Current cloud chemical models predict a dependence of sulfate production on the droplet size distribution. However, the droplet dynamics in existing models does not account for the turbulence in clouds. Therefore, a focus of our research concerning the heterogeneous chemistry in clouds will be to quantify the sulfate production of clouds including the process of turbulent coagulation. In this context, it will be worthwhile to implement the cloud parcel model in a more comprehensive atmospheric model, such as a full 3D Large Eddy Simulation (LES) model, which provides the meteorological input data for the cloud microphysics model, and includes transport and coupling with atmospheric chemistry.

REFERENCES

ARENBERG, D. 1939 Turbulence as the major factor in the growth of cloud drops. *Bull. Amer. Meteor. Soc.* **20**, 444 – 448.

BEARD, K. & OCHS, H. 1993 Warm-rain initiation: An overview of microphysical mechanisms. *J. Appl. Meteorol.* **32**, 608 – 625.

BELIN, F., MAURER, J., TABELING, P. & WILLAIME, H. 1997 Velocity gradient distri-

butions in fully developed turbulence: An experimental study. *Phys. Fluids* **9**, 3843 – 3850.

BERRY, E. 1967 Cloud droplet growth by collection. *J. Atmos. Sci.* **24**, 688 – 700.

BOTT, A. 1998 A flux method for the numerical solution of the stochastic collection equation. *J. Atmos. Sci.* **55**, 2284 – 2293.

BRENGUIER, J.-L. & CHAUMAT, L. 2001 Droplet spectra broadening in cumulus clouds. Part I: Broadening in adiabatic cores. *J. Atmos. Sci.* **58**, 628 – 641.

BUTUIRAT, F. & KIELKIEWICZ, M. 1996 On additivity of coagulation kernels. *Ann. Nucl. Energy* **23**, 1091 – 1096.

DHANIYALA, S. & WEXLER, A. 1996 Numerical schemes to model condensation and evaporation of aerosols. *Atmos. Env.* **30**, 919 – 928.

HALL, W. 1980 A detailed microphysical model within a two-dimensional dynamic framework: Model description and preliminary results. *J. Atmos. Sci.* **37**, 2486 – 2507.

JONAS, P. & GOLDSMITH, P. 1972 The collection efficiencies of small droplets falling through a sheared air flow. *J. Fluid Mech.* **52**, 593 – 608.

KOSTINSKI, A. & SHAW, R. 2001 Scale-dependent droplet clustering in turbulent clouds. *J. Fluid Mech.* **434**, 389 – 398.

KRUIS, F. & KUSTERS, K. 1997 The collision rate of particles in turbulent flow. *Chem. Eng. Comm.* **158**, 201 – 230.

MACPHERSON, J. & ISAAC, G. 1977 Turbulent characteristics of some Canadian cumulus clouds. *J. Appl. Meteorol.* **16**, 81 – 90.

MAXEY, M. 1987 The gravitational settling of particles in homogeneous turbulence and random flow fields. *J. Fluid Mech.* **174**, 441 – 465.

NEIZVESTNY, A. & KOBZUNENKO, A. 1986 Effect of small scale turbulence on the coagulation growth rate of cloud droplets. *Izv. Atm. Ocean. Phys.* **22**, 481 – 487.

PAOLI, R. & SHARIFF, K. 2004 Direct numerical simulation of turbulent condensation in clouds. Annual Research Briefs, Center for Turbulence Research, NASA AMES/Stanford Univ.

PARK, S., KRUIS, F., LEE, K. & FISSAN, H. 2002 Evolution of particle size distributions due to turbulent and Brownian coagulation. *Aerosol Sci. Technol.* **36**, 419 – 432.

PINSKY, M. & KHAIN, A. 1997 Turbulence effects on droplet growth and size distribution in clouds — A review. *J. Aerosol Sci.* **28**, 1177 – 1214.

PINSKY, M., KHAIN, A. & SHAPIRO, M. 1999 Collision of small drops in a turbulent flow. Part I: Collision efficiency. Problem formulation and preliminary results. *J. Atmos. Sci.* **56**, 2585 – 2600.

PINSKY, M., KHAIN, A. & SHAPIRO, M. 2000 Stochastic effects of cloud droplet hydrodynamic interaction in an turbulent flow. *Atmos. Res.* **53**, 131 – 169.

PRUPPACHER, H. & KLETT, J. 1997 *Microphysics of Clouds and Precipitation*. Kluwer Academic Publishers.

READE, W. & COLLINS, L. 2000 Effect of preferential concentration on turbulent collision rates. *Physics of Fluids* **12**, 2530 – 2540.

RIEMER, N. & WEXLER, A. 2004 Droplets to drops by turbulent coagulation. *J. Atmos. Sci.* Accepted for publication.

ROGERS, R. & YAU, M. 1989 *A Short Course in Cloud Physics*. Butterworth-Heinemann.

SAFFMAN, P. & TURNER, J. 1956 On the collision of drops in turbulent clouds. *J. Fluid Mech.* **1**, 16 – 30.

SQUIRES, K. & EATON, J. 1991 Preferential concentration of particles by turbulence. *Phys. Fluids A* **3**, 1169 – 1179.

SUNDARAM, S. & COLLINS, L. 1996 Numerical considerations in simulation a turbulent suspension of finite-volume particles. *J. Comp. Phys.* **124**, 337 – 350.

SUNDARAM, S. & COLLINS, L. 1997 Collision statistics in an isotropic, particle-laden turbulent suspension I. Direct Numerical Simulations. *J. Fluid Mech.* **335**, 75–110.

VAILLANCOURT, P. & YAU, M. 2000 Review of particle-turbulence interactions and consequences for cloud physics. *Bull. Amer. Meteorol. Soc.* **81**, 285 – 298.

VOHL, O., MITRA, S., WURZLER, S. & PRUPPACHER, H. 1999 A wind tunnel study of the effects of turbulence on the growth of cloud drops by collision and coalescence. *J. Atmos. Sci.* **56**, 4088 –4099.

WANG, L.-P. & MAXEY, M. 1993 Settling velocity and concentration distribution of heavy particles in homogeneous isotropic turbulence. *J. Fluid Mech.* **335**, 27 – 68.

WANG, L.-P., WEXLER, A. & ZHOU, Y. 1998 Statistical mechanical description of turbulent coagulation. *Phys. Fluids* **10**, 2647 – 2651.

WANG, L.-P., WEXLER, A. & ZHOU, Y. 2000 Statistical mechanical description and modelling of turbulent collision of inertial particles. *J. Fluid Mech.* **415**, 117 – 153.

WOODS, J., DRAKE, J. & GOLDSMITH, P. 1972 Coalescence in a turbulent cloud. *Q. J. R. Meteorol. Soc.* **99**, 758 – 763.

ZHOU, Y., WEXLER, A. & WANG, L.-P. 2001 Modelling turbulent collision of bidisperse inertial particles. *J. Fluid Mech.* **433**, 77 – 104.